

Operation of a Carbon Nanotube Field Emitter Array in a Hall Effect Thruster Plume Environment

Lake A. Singh, Graham P. Sanborn, Stephan P. Turano, Mitchell L. R. Walker,
and William Jud Ready, *Senior Member, IEEE*

Abstract—The Hall effect thruster is an electric propulsion device for space applications that efficiently reduces the propellant mass requirements on a spacecraft in comparison with chemical rockets. To date, the Hall effect thruster technology relies on the thermionic cathodes that consume up to 10% of the total propellant used in the system to neutralize the ion beam of the thruster; however, such propellant usage does not contribute to thrust generation. An array of thin-film, carbon nanotube field emitters that emit electrons through field emission can potentially neutralize the ion beam without consuming any propellant. This paper examines the effects of 40 min exposure of carbon nanotube field emitter arrays to the plasma environment in the exit plane of a Hall effect thruster. The physical structures that enable field emission appear largely unaffected by placement in the plasma as well as operation in the plasma. This indicates that a refined design of this carbon nanotube field emitter array may potentially provide an alternative to the thermionic cathode used on contemporary Hall effect thrusters and verifies that no fundamental incompatibilities exist between these two technologies.

Index Terms—Carbon nanotube (CNT), field emission (FE), Hall effect thruster (HET).

I. INTRODUCTION

HALL effect thrusters (HETs) have been used for several decades by space vehicles for station keeping and orbital maneuvering [1]. HETs ionize and accelerate propellant electrostatically, resulting in a high-velocity beam of ions. The HET requires a cathode to neutralize the ion beam to prevent spacecraft charging.

The present state-of-the-art cathode used in HETs is the thermionic or hollow cathode, which emits electrons from

Manuscript received December 27, 2013; revised May 6, 2014 and July 23, 2014; accepted September 2, 2014. This work was supported in part by the Georgia Tech Research Institute, Atlanta, GA, USA, in part by the High-Power Electric Propulsion Laboratory, Georgia Institute of Technology, Atlanta, GA, USA, in part by the U.S. Air Force Space and Missile Systems Center under Contract N00178-06-D-4752-FG01, and in part by the Defense Advanced Research Projects Agency under Contract HR0011-07-C-0056 and Contract HR0011-09-C-0142.

L. A. Singh and M. L. R. Walker are with the School of Aerospace Engineering, Georgia Institute of Technology, Atlanta, GA 30332 USA (e-mail: lake1@gatech.edu; mitchell.walker@ae.gatech.edu).

G. P. Sanborn and W. J. Ready are with the Georgia Tech Research Institute, Atlanta, GA 30332 USA, and also with the School of Materials Science and Engineering, Georgia Institute of Technology, Atlanta, GA 30332 USA (e-mail: graham.sanborn@gtri.gatech.edu; jud.ready@gtri.gatech.edu).

S. P. Turano is with the Georgia Tech Research Institute, Atlanta, GA 30332 USA (e-mail: stephan.turano@gtri.gatech.edu).

Color versions of one or more of the figures in this paper are available online at <http://ieeexplore.ieee.org>.

Digital Object Identifier 10.1109/TPS.2014.2357337

a heated surface. Thermionic cathodes ionize propellant to amplify the number of electrons extracted from the cathode to achieve the emission current required to neutralize the HET ion beam. The cathode propellant flow is not accelerated by the thruster to contribute to the thrust and can account for as much as 10% of the total propellant required by the thruster [2]. In contrast, field emission (FE) cathodes do not consume propellant. The primary consequence of this is up to a 10% increase in system-specific impulse. A secondary consequence is a reduction in the propulsion system power requirements by reducing the power the cathode system consumes through removal of the heater required by a thermionic cathode. This reduction in power is enabling for Cubesat applications. In this paper, we examine the effects of the HET plume environment on carbon nanotube (CNT) field emitter array (CFEA) technology to evaluate its potential as an alternative to the thermionic cathode on low-power HETs. CFEA devices are exposed to a thruster plume for 40 min and emission from said devices is attempted for 5 min. A short exposure time is selected, because this is the first attempt at integrating these technologies.

A. Carbon Nanotube Field Emission

The discovery of CNTs is credited to Iijima in 1991, although CNTs may have been synthesized as early as 1889 [3], [4]. CNTs, namely multiwall CNTs (MWNT), tend to behave as electrical conductors [5]. MWNTs have other properties such as an atomically sharp tip, whiskerlike geometry, chemical inertness, and thermal stability, thus making them attractive for field emission (FE) applications [6].

FE is a fundamentally different phenomenon of emission of electrons from a material compared with thermionic emission, employed in present state-of-the-art hollow cathodes. Thermionic electron emission overcomes the potential barrier of the electronic structure of the material by supplying sufficient thermal energy to the electrons [7]. In contrast, FE overcomes the potential barrier by using an electric field on the order of $10\text{--}10^2$ V/ μm to lower the potential barrier enough such that the probability of electrons to quantum mechanically tunnel through the barrier becomes significant [8]. FE is achievable at room temperatures, but the high electric fields required to realize emission leads to geometry and material selection considerations dominating the design space.

The high electric fields required for FE can be attained via a combination of large potential differences and small spacing.

In the limit of minimizing both the potential and the size of the device, electrode spacing is taken to the microscopic level, and the large electric fields are realized through clever geometry.

Normally, large electric fields ($100 \text{ s of } V \mu\text{m}^{-1}$) are needed for FE [9], but this field is highly dependent on the electron source geometry, where sharp tips enhance the macroscopic electric field. These FE sources can be much more efficient and reliable, if emission can be achieved at a sufficiently low potential, providing marked improvement over current technologies [6], [10], [11]. Conductive, high aspect ratio nanomaterials, such as CNTs, have this favorable geometry for improving FE performance by field enhancement. CNTs are ideal for FE, having very high electrical conductivity, high temperature stability, chemical inertness, and a nanoscale high aspect ratio [12]–[14].

The seminal work in this type of FE design is due to Spindt in 1968, and cathodes of this type are typically referred to as Spindt FE cathodes [15]. Spindt cathodes incorporate arrays of emission tips with an internal gate electrode by using silicon microfabrication techniques. Spindt FE tips were historically metal cones whose tips are a few hundred nanometers in diameter and recessed underneath the gate electrode. A bias between the FE tips and the gate electrode produces the high electric field necessary to enable FE from the tips. The Spindt design [11] attains high current densities by tightly packing a large number of electrostatically isolated emitting elements.

The metal cones used in traditional Spindt cathodes have drawbacks that CNTs do not share. The metal tips can interact chemically with the ambient environment, which can change the electronic structure of the emitting material and inhibit further emission. An HET plasma environment also subjects the metal tips of Spindt cathodes to sputtering from the plasma, which leads to erosion that can permanently degrade their performance at a rate that far exceeds the degradation of the thruster [16]. In contrast, carbon has a much lower sputtering rate than the metals used for traditional Spindt cathodes [17]. The bond structure of the CNT makes them far less reactive than metal [12]. Additionally, CNTs do not suffer from performance degradation through erosion as a result of their whiskerlike geometry, which does not experience appreciable tip blunting from erosion [18].

B. CNT FE Array Design

The details of the CNT electron source specifically designed to prevent shorting of the gate layer has been reported elsewhere [19]. In this design, etch pits extend into the Si substrate, and isotropic etching is utilized to create a vertical and lateral buffer zone between the gate and CNTs, respectively. Doped silicon serves as the substrate and cathode contact [19]. Thermally grown SiO_2 about $2 \mu\text{m}$ thick is used as the insulator, and 500-nm-thick doped polycrystalline silicon (p-Si) is used as the gate [19]. Fig. 1 shows a schematic of the fabrication process. Standard ultraviolet lithography is used to pattern the substrate [Fig. 1(c)]. Arrays of $4\text{-}\mu\text{m}$ diameter circles across an $8.5 \text{ mm} \times 8.5 \text{ mm}$ square with a 50, 100, or $200 \mu\text{m}$ pitch are patterned on each die. These pitch

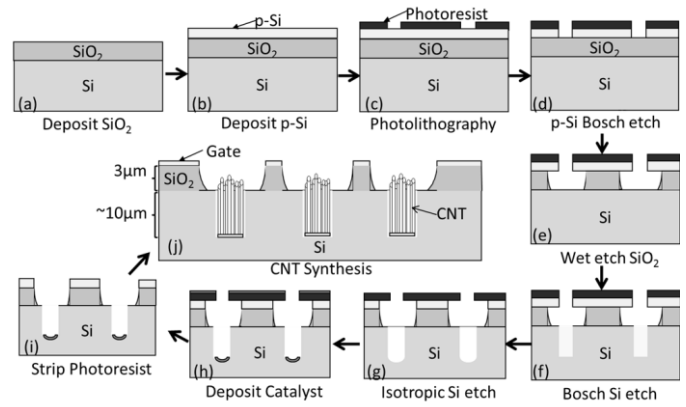


Fig. 1. Fabrication process flow for the internally gated CNT FE design components (a)–(j) represent sequential stages in the fabrication process.

and feature diameters have not yet been optimized to maximize performance.

A Bosch etch process anisotropically etches the p-Si gate [Fig. 1(d)], and the SiO_2 is isotropically etched in a buffered oxide etch solution [Fig. 1(e)]. A second Bosch etch is used to deepen the etch pits by etching into the Si substrate [Fig. 1(f)]. An SF_6 reactive ion etch process simultaneously removes the undercut p-Si and increases the diameter of the Si pit [Fig. 1(g)]. The etch geometry allows for electron beam evaporation of the Fe catalyst directly on the base of the pit [Fig. 1(h)]. A low-pressure chemical vapor deposition (LPCVD) system with precisely controlled process parameters is used to produce uniform and consistent CNT growth [Fig. 1(j)]. The LPCVD synthesis uses C_2H_2 and NH_3 or H_2 at $700 \text{ }^\circ\text{C}$ and 10 mbar for $0.5\text{--}5 \text{ min}$. The CNT growth can be precisely controlled, remains aligned past the Si pit, and is uniform across many pits [19].

The substrate and CNT structures comprise the cathode electrode and are referred to as such throughout this paper. This CFEA design field emits when the cathode electrode is biased negatively with respect to the gate electrode. Typical performance of these devices can be found in [19].

II. EXPERIMENTAL SETUP

A. Thruster Cathode Array Design

A Kyocera gold-plated, plug-in, hybrid bathtub-type package provides the interface between the CFEA and the rest of the test circuit. These packages form a cost effective way of integrating the delicate CFEA device into experimental setups. Each package is cut in half to reduce its footprint. Fig. 2 shows one CFEA installed on a package. Ablebond 84-ILMI heat cure silver epoxy binds the cathode to the base of the package, which establishes the electrical and mechanical connection between the package base and cathode. Wire bonds form high-quality ($<1 \Omega$) connections between the package and the chip by redundantly connecting package pins to the gate on the CFEA and the package base.

The thruster cathode array mechanically and electrically integrates up to 80 packages of CFEAs into a single device for reliable interface to the HET and experimental setup. Fig. 3 shows an exploded view of the array design, and Fig. 4

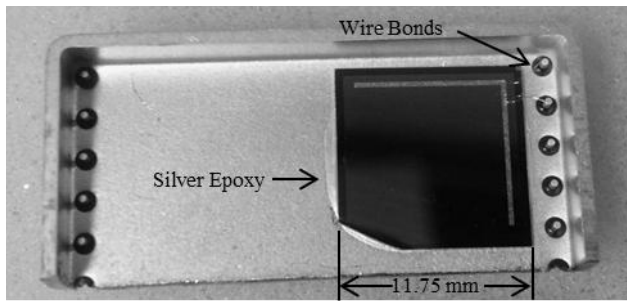


Fig. 2. CFEA emitter chip installed onto a package with silver epoxy.

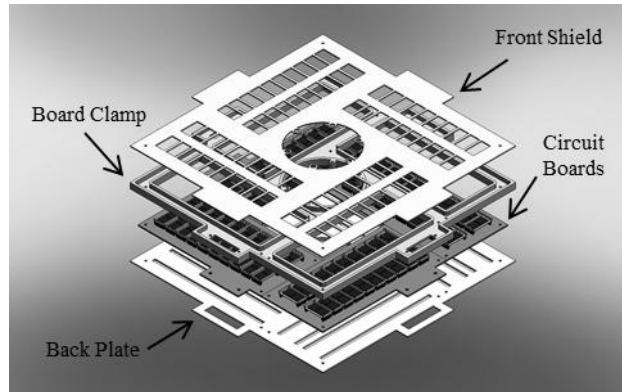


Fig. 3. Exploded view of the thruster cathode array design. The four major components of the array are visible in this view.

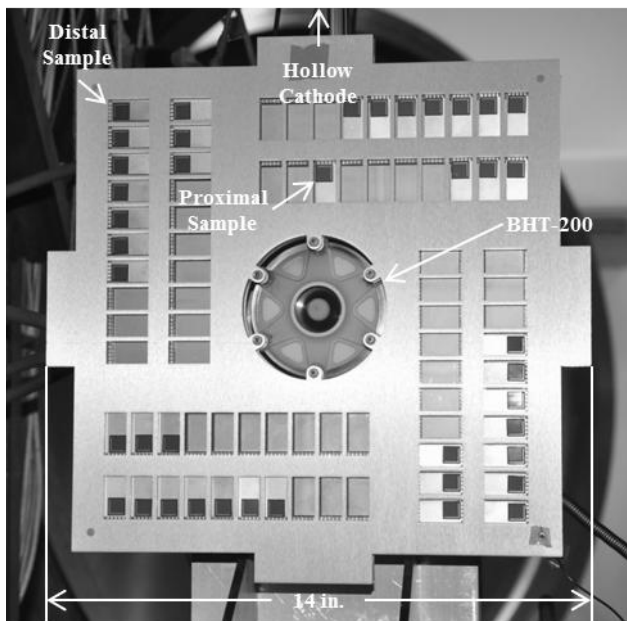


Fig. 4. Thruster cathode array with CFEAs installed and integrated onto a BHT-200 HET. The hollow cathode is located beyond the upper border of the image.

shows the constructed array. The rigid, detachable array can be reused on subsequent experiments, can survive the near-thruster plasma environment, and is light enough not to require additional support when fixed to the HET.

Four identical circuit boards in the array can each accommodate 20 packages. The circuit boards connect all gate

electrodes on the installed CFEAs to a common ground plane on the bottom layer of the board and connect each cathode electrode to an independent pin on a DB-25 connection installed on the board. This architecture facilitates independent data collection on the cathode electrode channels for each installed CFEA and would not be necessary on a flight device. All connections are made through the package pins. A 3/16 in machined aluminum back plate provides mechanical support for the circuit boards and forms the base of the array. The side of the aluminum plate interfacing with the circuit boards electrically connects to the ground plane on the bottom of the boards. Channels cut into this side of the plate ensure that the circuit boards can sit flush against the plate without undesirable electrical connections with the solder connections on the boards. The opposing side of the plate is anodized to prevent interference from the plasma environment around the thruster.

A machined G-10 plate (the board clamp) rests on the opposite side of the circuit boards from the back plate and mechanically secures the circuit boards to the back plate. It also provides space between the circuit board surface and an anodized aluminum front shield that obscures sensitive parts of the array from the plasma environment near the thruster. The thruster cathode array interfaces with a Busek BHT-200 200-W HET via the six radially arranged bolt holes located in the center of the array [20]. Alumina spacers installed in the face of the HET electrically isolate the thruster cathode array from the HET during operation. Previous experiments with CFEAs of this design indicated they would have insufficient performance to start and maintain the thruster on their own. The BHT-200 requires 1 A of cathode current to nominally operate while the nominal performance of 39 CFEAs as presently designed would produce at most 39 mA of electron current. A Moscow Aviation design hollow cathode mounted separately performs the function of operating the thruster.

Fig. 4 shows the placement of 41 CFEAs in the thruster cathode array, including two defective devices. A full complement of CFEAs was not installed, because it was not necessary for the goals of this paper. Most CFEAs were positioned in the furthest radial locations from the HET (located in the center of the array) in an effort to capture the effects of the plume on the CFEAs while minimizing the risk of catastrophically damaging them. Two of the cathodes were included despite manufacturing defects. One of the nonfunctional cathodes was positioned in the closest radial position (the proximal sample) and the other was positioned in the furthest radial position (the distal sample) to determine the effects of the plasma on a nonfunctioning CFEA. Both nonfunctional CFEAs were imaged under SEM prior to installation in a repeatable way so that identical emission features could be observed both before and after exposure to the HET plasma.

B. Test Circuitry

The data acquisition system developed for this paper biases the cathode electrodes in parallel via a common power supply. Each independent cathode channel includes a current shunt and switch to isolate failed or defective CFEAs from the

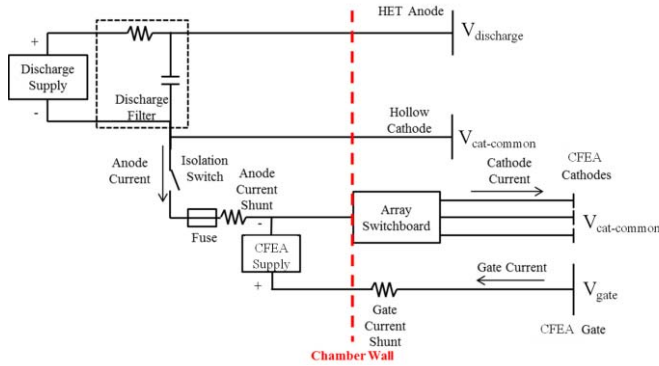


Fig. 5. Full HET test circuit. The HET circuit (top portion) connects to the CFEA circuit (bottom portion) via the HET discharge negative line.

rest of the circuit. A National Instruments PXI-1033 data acquisition chassis equipped with two PXI-2567 external relay driver modules, two PXI-2527 multiplexer modules, and one PXI-4065 digital multimeter module gathers the data from each of the current shunts during testing. The system records data once every 15 s.

The test circuit shown in Fig. 5 integrates the standard HET circuit with a thermionic hollow cathode and the thruster cathode array test circuit. The discharge power supply biases the anode of the HET and establishes the floating low potential of the full system circuit. Sharing the discharge low potential with the discharge power supply for the HET, the Moscow Aviation hollow cathode heater, and keeper power supplies drive the operation of the thermionic cathode. This common potential is referred to as the hollow cathode common potential. The hollow cathode common potential connects to the cathode electrode side of the thruster cathode array circuit to make the connection between the two subcircuits. Between the CFEA power supply and the cathode electrodes lies a component titled Array Switchboard which serves to isolate each cathode electrode onto its own parallel circuit and measure current. The National Instruments data acquisition unit interfaces with the Array Switchboard to control the array and acquire the measured current data. Current data is tabulated such that positive values represent electron flow in the designed direction. Fig. 5 shows arrow indicators which prescribe the direction of electron flow for positive current data.

Some additional components added into the circuit protect thruster cathode array components from HET transients during operation. The first protective measure is a normally open isolation switch. It is closed once the HET is operating in steady-state and the test is ready to begin. The second line of defense is a 315 mA fuse that blows, if an overcurrent condition develops in the HET circuit. Previous publications detail the standard triode mode of operation of the CFEA devices [19]. In this circuit configuration, the gate electrode is biased positively with respect to the cathode electrodes, which float at the HET negative discharge potential. The anode of the HET serves as the anode electrode component for the triode configuration, and is biased above both the gate and cathode electrodes. Positive cathode current is defined

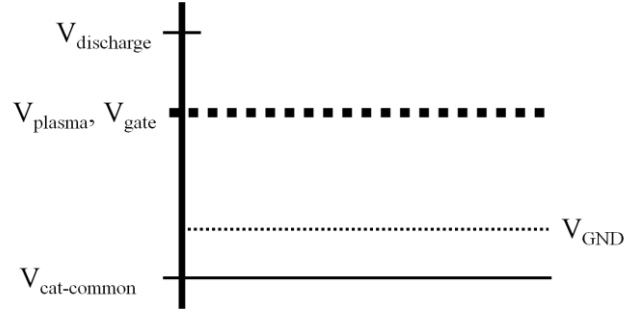


Fig. 6. Ideal potential diagram for a CFEA/hollow cathode-coupled HET setup.

to be electrons emitting from the electrode, whereas positive gate current is defined to be electrons arriving to the electrode. Positive anode current is defined to be electrons traveling from the HET subcircuit to the CFEA subcircuit.

The potential diagram in Fig. 6 shows the ideal placement of electric potentials in the system relative to one another. The HET discharge potential should be the anode of the system. Both the hollow cathode common potential and the CFEA cathode potential form the cathode. The plasma potential in the thruster exit plane and the CFEA gate potential are between both the system anode and cathode. Ideally, the gate potential should be at or slightly below the plasma potential to prevent the back-streaming of hollow cathode electrons to the gate electrode. However, the potential difference between the plasma potential and the cathode common potential is insufficient to produce FE from the CFEAs used in this paper. As a result, the gate potential exceeds the plasma potential during the emission test portion of this experiment.

The VTF-2 facility at the Georgia Tech High-Power Electric Propulsion Laboratory houses the experiment and produces a base pressure of 1×10^{-9} torr before HET operation begins. The chamber maintains a pressure of 1.1×10^{-6} torr-Xe near the chamber wall during HET operation.

III. RESULTS AND DISCUSSION

A. Emission Test Data

Fig. 7 shows the thruster cathode array current and applied potential data as a function of time over the duration of the emission test portion of the experiment. The collected data can be broken up into three distinct stages according to how the emission test was conducted. Before data collection, the HET was brought to a nominal operating point with 200 V discharge voltage and 1.05 A discharge current. Empirical data from previous researchers demonstrates that the plasma potential in the CFEA-occupied region of the exit plane is ~ 10 V, and the plasma density is $\sim 4 \times 10^{16} \text{ m}^{-3}$ [21], [22]. The isolation switch between the HET and CFEA subcircuits was open at this time. Once the HET was operating stably, the data acquisition program began capturing data and the isolation switch was closed. This event occurred 10 min into HET operation, and integrated the CFEA subcircuit into the HET subcircuit. The data acquisition system measured baseline data for the circuit with the CFEAs unbiased for 2 min

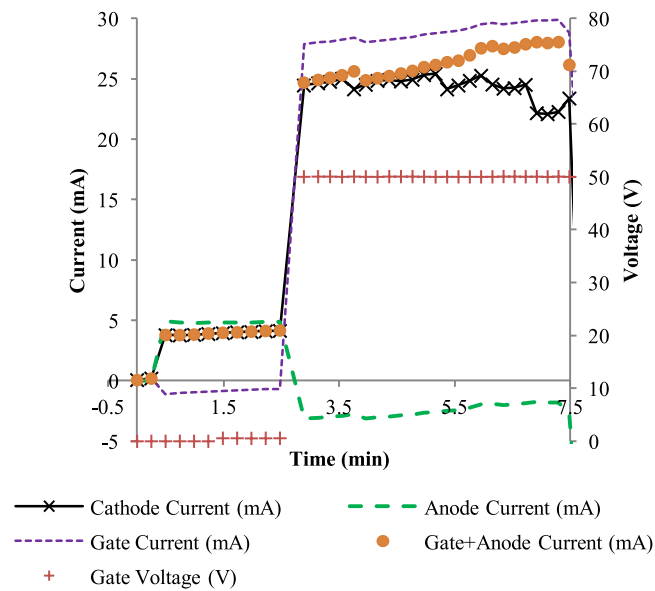


Fig. 7. Full thruster cathode array current data.

before biasing the CFEAs. Once the CFEAs were biased, the system operated for 5 min before all CFEAs appeared to be shorted. Data acquisition ended at this point. As stated previously, this 5 min emission test occurred during the 40 min exposure to the HET environment reported in this paper.

The first stage covers the first two data points. The isolation switch connecting the HET and CFEA circuits is open during this stage. Consequently, no current travels between the CFEA circuit and HET circuit (stated as anode current). There are 68–200 μA of gate and cathode current during this period. The HET was already running at steady-state at the beginning of the test, so the current is likely noise from the charge exchange (CEX) ion and hollow cathode electron collisions.

The second stage consists of the next 9 data points. The isolation switch is closed at the beginning of this stage, but the CFEA power supply has not started outputting. Power supply output starts during the middle of the second stage, as seen by the small jump in gate voltage from 0 V to 0.575 V. Negative gate current, and positive anode and cathode currents result from closing the switch. The currents detected correspond with CEX and hollow cathode ions bombarding the CFEA and electronics package surfaces, which are now set to the hollow cathode common potential on the HET circuit instead of the floating potential.

The third stage consists of the large positive plateau, and is where field emission was actually attempted. At this point, the gate potential rises to +50 V from the cathode potential, which is still equal to the hollow cathode common potential (about -10 V).

A previous publication details typical performance of the CFEA technology used in this paper [19], and reveals limited cathode current density ($<50 \mu\text{A}/\text{cm}^2$) at a bias of 50 V. In contrast, the measured cathode current from this test equates to a current density of roughly $650 \mu\text{A}/\text{cm}^2$. The order of magnitude difference in documented performance provides evidence that charged particles from the plasma and electrical shorting form the primary contributions to the

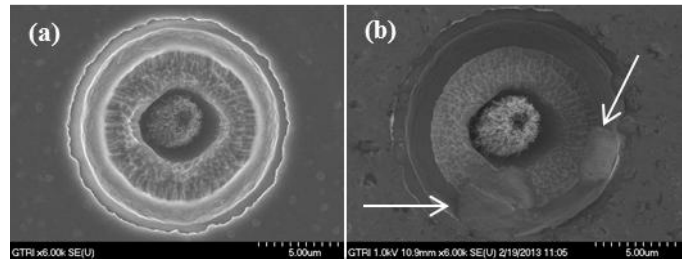


Fig. 8. (a) Before and (b) after SEM images of the same emission feature from the distal sample. Arrows in (b) point to particulate debris present in the feature after exposure to the HET environment.

measured currents. A large positive gate current results from electrons from the hollow cathode colliding with the gate which is biased above the floating potential. Enough electrons arrive at the gate that they reverse the desired direction of current between the HET and CFEA subcircuits. This effect is manifested as a negative anode current. There is also positive cathode current, which corresponds with CEX and hollow cathode ions colliding with the exposed package areas as shown in Fig. 2. The gate + anode current values diverge from the cathode current because the experiment software stopped acquiring cathode current data on some channels even though they were still active. Insufficient performance of the CFEAs at low voltage and the presence of a hollow cathode combine to introduce significant interference into the collection of FE current data in this experiment.

B. Before and After SEM Comparison

The proximal and distal nonfunctioning CFEA samples underwent repeatable SEM imaging both prior to and after HET exposure. This imagery provides a means to look for any catastrophic physical damage to the emission features on the CFEAs from exposure to the plasma environment. Fig. 8 shows a single emission feature on the distal sample prior to [Fig. 8(a)] and after [Fig. 8(b)] the HET test. Close examination reveals the overall structure to be identical between the two images, with two exceptions. The post-exposure image shows some particulate debris present in the emission feature marked with arrows. Both the proximal and distal samples have a few features with similar debris accumulation, but most features appear unchanged in the before/after imagery. This particulate debris could be from spallation of part of the array. The debris could also be from handling the devices between the two images when they were unavoidably transported outside of a clean room environment for testing.

The before and after images in Fig. 8 also reveal a difference in contrast between polysilicon grains on the gate electrode. This difference is likely attributable to a change in operating voltage on the SEM between the two images and charging of the gate electrode. The SEM operating voltage is at 1 kV lower in Fig. 8(b) as opposed to 10 kV because the CFEA is not removed from the electronic package after the test to avoid damage to the CFEA during removal. SEM images from before HET testing were taken without the package to achieve maximum resolution and contrast. Unfortunately, the lower operating voltage results in poor image contrast and

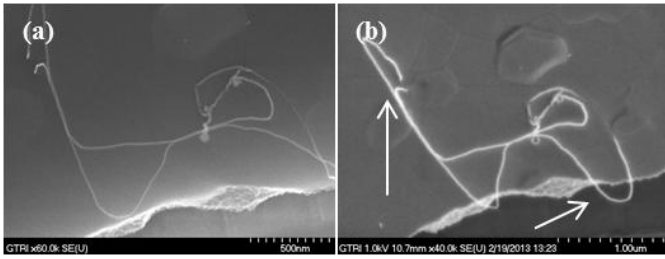


Fig. 9. (a) Before and (b) after images of the same stray CNT on the polysilicon surface of the distal sample. The CNT has moved slightly between imaging sessions.

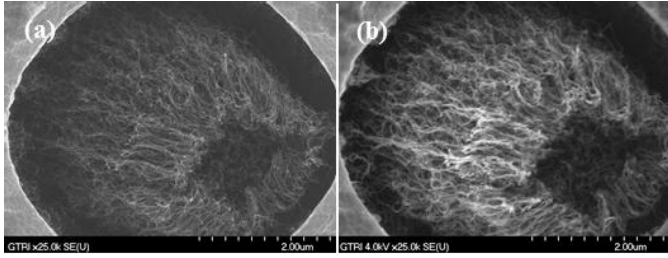


Fig. 10. (a) Before and (b) after images of the same CNT bundle on the proximal sample. The CNT bundle appears to be unaffected by exposure to the HET environment.

lower resolution. However, the image quality is sufficient to allow for identification of catastrophic damage to emission features. None of the features on the distal or proximal samples showed evidence of catastrophic damage, indicating no effect to the CFEA from short-term exposure to the HET environment.

Fig. 9 shows a fortuitously mis-grown CNT on the polysilicon surface of the distal sample before [Fig. 9(a)] and after [Fig. 9(b)] HET exposure. The position of the CNT remains largely unaffected between the two images, but some changes are present. In particular, the part of the CNT in the upper left of both images appears to have flipped or twisted, while the component of the CNT on the lower right of the image appears to have untwisted and dropped slightly into the nearby etched pit. These changes in position could be due to HET exposure or to handling during the installation and removal of the distal sample from the thruster cathode array. Previous studies report motion of CNTs under the presence of electric fields and during FE [18]–[23]. While this CNT cannot have performed FE, it was exposed to the HET plasma and the electric field variations present at its length scale could be responsible for this observed behavior. A more detailed analysis of this effect is beyond the scope of this paper.

Fig. 10 shows a single CNT bundle on the proximal sample before [Fig. 10(a)] and after [Fig. 10(b)] HET exposure. Like most emission features on the CFEAs exposed to the HET environment, there are no observable changes in the emitter geometry after exposure. Close examination of these images reveals no observable differences in the polysilicon gate, the SiO_2 insulator, the silicon substrate, or the CNTs. The remarkable similarity between the two images in Fig. 10 proves that CFEA technology can survive short-term exposure to a near HET environment when not biased and shielded by the gate electrode. Fig. 11 extends this result to functioning,

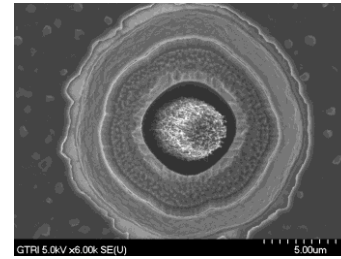


Fig. 11. SEM image of a single emission feature on a CFEA which was biased while inside the HET environment. The emission feature appears undamaged after operation in the HET environment.

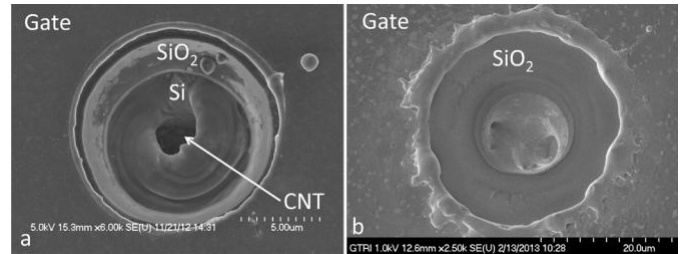


Fig. 12. Two emission features which suffered arcing failure during the experiment. (a) demonstrates damage to the substrate and (b) demonstrates damage to both the substrate and gate.

shielded emission features by indicating no damage after exposure to the HET environment when compared with a similar structure in Fig. 8(a).

C. Arcing and Sputtering

While most emission features on the CFEAs appear unaffected by short-term exposure to the HET environment, arcing failure between the gate and cathode electrodes which has been observed outside of a HET environment still occurs on some features. Fig. 12 shows two emission features which have experienced arcing failure with melting of the gate and the interior of the feature. Arcing leads to melting and distinct changes in emission feature geometry as evident in Fig. 12. Additionally, significant sputtering of the gold plating on the electronic packages resulted in shorts developing on some packages between the package body and gate electrode pins. These shorts are due to the sputtered gold adhering to the insulation between the gate electrode pins and the package body, thus creating an electrically conductive pathway. Notably, no sputtered gold was detected on the CFEA devices themselves. Although unfortunate and unintended, the sputtered gold reveals important information regarding the performance of the CFEAs in the HET environment.

The symmetry of the array allows for CFEAs placed in the same slot across different quadrants to be treated together. Fig. 13 shows the number of occurrences of arcing failure and gold sputter failure across the thruster cathode array. The number on the top in each slot indicates the number of electronic packages that shorted from sputtered gold, whereas the number on the bottom indicates the number of CFEAs that failed from arcing between the cathode and gate electrodes. In this depiction, the BHT-200 lies beyond the left side of the image. Sputter failure was confirmed by spectroscopy

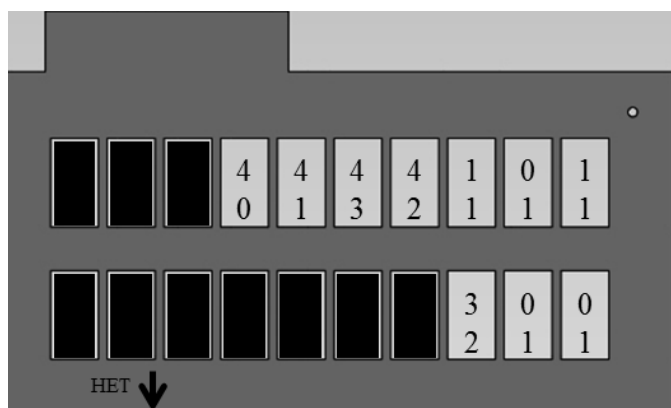


Fig. 13. Schematic of one quadrant of the thruster cathode array. The numbers on the top of each CFEA location indicate the number of packages in this slot around the array that shorted from sputtered gold, whereas the number on the bottom indicates the number of CFEAs that suffered failure from arcing.

of the pin insulation whereas arc failure was confirmed by testing the resistance of the CFEA after removal of the wire bond.

Plotting the sputtering short data in this manner reveals a clear transition from packages which shorted due to sputtering at positions close to the HET to packages that did not short due to sputtering far from the HET. Careful examination of the insulation on the electronic packages reveals that all packages experienced sputtering, although some packages did not experience sufficient sputtering to create a conductive pathway. The amount of material sputtered is a function of the incident energy of the ions, the binding energy of the sputtered material, the relative atomic masses, and the number of incident ions [24]. Since significant sputtering still occurred on the farthest packages, it is likely that variation in the ion density is responsible for the noted transition. Also of note, the quadrant of the array which was closest to the hollow cathode did not have any observable differences compared with the other three quadrants.

The sputtering shows variation with distance from the HET as a result of variation in the ion density, but the frequency of arcing failure does not share this variation. This indicates that the variation in the ion density does not significantly alter the likelihood of an arc failure occurring on a CFEA sample. The positively biased gate electrode present during emission likely shields the emission feature from incident ions, thus removing their contribution to this failure mode.

IV. CONCLUSION

This paper has led to three major findings. Significant interference from the local plasma environment prevented accurate measurement of FE current. Insufficient performance at low voltage and the necessary presence of the hollow cathode led to this result. Future work to optimize the design of the CFEA devices used in this paper will improve low voltage performance and ultimately remove the need for a coupled hollow cathode. Together, these developments will allow for operation of the CFEAs with the HET in the ideal manner discussed in the experimental setup.

The experiment in this paper experienced unanticipated sputtering of gold from exposed areas of the electronics packages used to integrate the CFEAs to the test apparatus. Observation of the pattern of sputtering across the array led to the discovery that ion density plays no significant role in the rate of arcing failure the CFEAs experience. This is likely due to shielding of the emission features by the positively biased gate electrode.

Ultimately, this paper sought to determine the short-term survivability of the CFEA technology in an HET environment and identify any fundamental incompatibility between the two technologies. Despite the limitations in the work, the results present useful insight into the operation of a HET with CFEA cathodes which satisfies this objective. Before and after SEM imaging of the closest and farthest placed CFEAs from the thruster confirm that CFEAs can exist in the HET environment. CFEA samples which were energized in the emission test showed no enhanced rate of arcing when compared to samples previously tested outside the HET environment. While there are unquestionably numerous refinements to be made both to the CFEA and thruster cathode array designs, that these devices can withstand being near a thruster is encouraging for continued development.

REFERENCES

- [1] V. Kim *et al.*, "Electric propulsion activity in Russia," in *Proc. Int. Electr. Propuls. Conf.*, Pasadena, CA, USA, 2001, paper IEPC-7.
- [2] D. L. Tilley, K. H. de Grys, and R. M. Myers, "Hall thruster-cathode coupling," in *Proc. 35th AIAA/ASME/SAE/ASEE Joint Propuls. Conf. Exhibit*, Los Angeles, CA, USA, 1999, paper IEPC-7.
- [3] S. Iijima, "Helical microtubules of graphitic carbon," *Nature*, vol. 354, pp. 56–58, Nov. 1991.
- [4] M. Monthioux and V. L. Kuznetsov, "Who should be given the credit for the discovery of carbon nanotubes?" *Carbon*, vol. 44, no. 9, pp. 1621–1623, 2006.
- [5] P. J. F. Harris, *Carbon Nanotube Science: Synthesis, Properties and Applications*. Cambridge, U.K.: Cambridge Univ. Press, 2009.
- [6] W. I. Milne *et al.*, "Carbon nanotubes as field emission sources," *J. Mater. Chem.*, vol. 14, no. 6, pp. 933–943, 2004.
- [7] O. W. Richardson, *The Emission of Electricity from Hot Bodies*. London, U.K.: Longmans, Green, and Company, 1921.
- [8] R. H. Fowler and L. Nordheim, "Electron emission in intense electric fields," *Proc. Roy. Soc. London A*, vol. 119, no. 781, pp. 173–181, 1928.
- [9] R. Gomer, *Field Emission and Field Ionization*. Cambridge, MA, USA: Harvard Univ. Press, 1961.
- [10] J. D. Carey, "Engineering the next generation of large-area displays: Prospects and pitfalls," *Philosoph. Trans. Roy. Soc. London A*, vol. 361, no. 1813, pp. 2891–2907, 2003.
- [11] C. A. Spindt, C. E. Holland, A. Rosengreen, and I. Brodie, "Field-emitter arrays for vacuum microelectronics," *IEEE Trans. Electron Devices*, vol. 38, no. 10, pp. 2355–2363, Oct. 1991.
- [12] A. Loiseau, P. Launois-Bernede, P. Petit, S. Roche, and J.-P. Salvetat, *Understanding Carbon Nanotubes: From Basics to Applications*, vol. 677. Berlin, Germany: Springer-Verlag, 2006.
- [13] W. I. Milne *et al.*, "Electrical and field emission investigation of individual carbon nanotubes from plasma enhanced chemical vapour deposition," *Diamond Rel. Mater.*, vol. 12, nos. 3–7, pp. 422–428, 2003.
- [14] W. A. de Heer, A. Châtelain, and D. Ugarte, "A carbon nanotube field-emission electron source," *Science*, vol. 270, no. 5239, pp. 1179–1180, 1995.
- [15] C. A. Spindt, "A thin-film field-emission cathode," *J. Appl. Phys.*, vol. 39, no. 7, pp. 3504–3505, 1968.
- [16] C. M. Marrese *et al.*, "Performance of field emission cathodes in xenon electric propulsion system environments," in *Micropropulsion for Small Spacecraft*, vol. 187, 1st ed. Reston, VA, USA: AIAA, 2000, pp. 271–302.
- [17] W. M. Stacey, *Fusion Plasma Physics*. Darmstadt, Germany: Wiley, 2005.

- [18] Z. L. Wang, R. P. Gao, W. A. de Heer, and P. Poncharal, "In situ imaging of field emission from individual carbon nanotubes and their structural damage," *Appl. Phys. Lett.*, vol. 80, no. 5, pp. 856–858, 2002.
- [19] G. Sanborn, S. Turano, P. Collins, and W. J. Ready, "A thin film triode type carbon nanotube field emission cathode," *Appl. Phys. A*, vol. 110, no. 1, pp. 99–104, Jan. 2013.
- [20] V. Hrubby, J. Monheiser, B. Pole, P. Rostler, and J. Kolencik, "Development of low power Hall thrusters," in *Proc. 30th Plasmadyn. Lasers Conf.*, Norfolk, VA, USA, 1999, paper JPC-9.
- [21] B. E. Beal, A. D. Gallimore, and W. A. Hargus, Jr., "Plasma properties downstream of a low-power Hall thruster," *Phys. Plasmas*, vol. 12, no. 12, p. 123503, 2005.
- [22] B. E. Beal, A. D. Gallimore, J. M. Haas, and W. A. Hargus, Jr., "Plasma properties in the plume of a Hall thruster cluster," *J. Propuls. Power*, vol. 20, no. 6, pp. 985–991, 2004.
- [23] Y. Saito, K. Seko, and J.-I. Kinoshita, "Dynamic behavior of carbon nanotube field emitters observed by *in situ* transmission electron microscopy," *Diamond Rel. Mater.*, vol. 14, nos. 11–12, pp. 1843–1847, 2005.
- [24] N. Matsunami *et al.*, "Energy dependence of the ion-induced sputtering yields of monatomic solids," *Atomic Data Nucl. Data Tables*, vol. 31, no. 1, pp. 1–80, 1984.



Lake A. Singh received the B.S. degrees in aerospace engineering and physics from the Virginia Polytechnic Institute and State University, Blacksburg, VA, USA, in 2009, and the M.S. degree in aerospace engineering from the Georgia Institute of Technology (Georgia Tech), Atlanta, GA, USA, in 2012, where he is currently pursuing the Ph.D. degree in aerospace engineering.

He was an Intern with the Aerospace Corporation, El Segundo, CA, USA, from 2007 to 2009. He also held an internship with Jacobs Engineering Group Inc., Pasadena, CA, USA, in support with the Marshall Space Flight Center, Huntsville, AL, USA, in 2013, where he was involved in improving models of the J-2X engine. He is currently a Graduate Research Assistant with the High-Power Electric Propulsion Laboratory, Georgia Tech. His current research interests include use of carbon nanotube field emitter arrays for electric propulsion, space debris remediation, and *in-situ* propellant collection.

Mr. Singh is a Student Member of the American Institute of Aeronautics and Astronautics.



Graham P. Sanborn received the B.S. degree in chemistry from Spring Hill College, Mobile, AL, USA, in 2009, and the M.S. degree in materials science and engineering from the Georgia Institute of Technology (Georgia Tech), Atlanta, GA, USA, in 2012, where he is currently pursuing the Ph.D. degree in materials science and engineering.

He was a Research Intern with the School of Materials Science and Engineering, Georgia Tech. He is currently a Graduate Research Assistant with the Carbon Based Materials Group, Georgia Tech Research Institute, Atlanta, for his thesis research. His current research interests include electronic applications of carbon nanomaterials and carbon nanotube composites.

Mr. Sanborn was a recipient of the Technological Innovation: Generating Economic Results Fellowship Award from Georgia Tech, the President's Scholar in Chemistry Award from Spring Hill College, and his team received the First Place Award at the 2013 Georgia Tech Business Plan Competition.

Stephan P. Turano received the B.S. and M.S. degrees in materials science and engineering from the Georgia Institute of Technology, Atlanta, GA, USA, in 2002 and 2005, respectively.

He was with the Materials Analysis Center, Georgia Tech Research Institute, Atlanta, from 2005 to 2007, where he was involved in failure analysis. From 2007 to 2009, he was a Research Engineer with Kawneer Company, Norcross, GA, USA, where he investigated advanced materials for energy efficient building envelopes. He is currently a Research Scientist with the Electro-Optic Systems Laboratory, Georgia Tech Research Institute. His current research interests include microelectromechanical systems device fabrication, thin-film photovoltaic materials, and electronic applications of carbon nanomaterials.

Mr. Turano is a member of the Minerals, Metals and Materials Society, where he serves on the Nanomaterials Committee. He has previously served in a leadership position in the Atlanta chapter of ASM.



Mitchell L. R. Walker received the B.S., M.S., and Ph.D. degrees in aerospace engineering from the University of Michigan, Ann Arbor, MI, USA, in 1999, 2000, and 2004, respectively. He is currently an Associate Professor with the School of Aerospace Engineering, Georgia Institute of Technology (Georgia Tech), Atlanta, GA, USA.

He was an Intern with Lockheed Martin Missiles and Space Systems, Denver, CO, USA, and Lockheed Martin Tactical Aircraft Systems, Fort Worth, TX, USA, from 1997 to 2000, and a Research Assistant with the Plasmadynamics and Electric Propulsion Laboratory, University of Michigan, from 2000 to 2004. In 2005, he joined Georgia Tech as an Assistant Professor. He has authored over 65 technical publications. His current research interests include electric propulsion, plasma physics, and hypersonic aerodynamics with plasma interaction.

Dr. Walker was selected as an American Institute of Aeronautics and Astronautics (AIAA) Associate Fellow in 2011. He was a recipient of the AIAA Lawrence Sperry Award in 2010 and the Air Force Office of Scientific Research Young Investigator Award in 2006.

William Jud Ready (M'04–SM'06) received the B.S., M.S., and Ph.D. degrees in materials science and engineering from the Georgia Institute of Technology (Georgia Tech), Atlanta, GA, USA, in 1994, 1997, and 2000, respectively.

He was with General Dynamics and MicroCoating Technologies, Inc., Atlanta, from 2000 to 2003. He is currently a Principal Research Engineer with the Georgia Tech Research Institute, Atlanta, and an Adjunct Professor with the School of Materials Science and Engineering, Georgia Tech. His current research interests include electronics reliability, carbon nanomaterials, neuronal prosthetics, photovoltaics, and supercapacitors.

Dr. Ready is a member of the Materials Research Society and serves on the board of TMS. He received the Outstanding Undergraduate Research Mentor Award from Georgia Tech in 2009, and the Young Leaders International Scholar Award from the Japan Institute of Metals and TMS in 2005.